Michele Stofella
Bifurcations Analysis of Morris Lecar Model for Excitability classification
Models and Numerical Methods

Contents

1 Introduction

Neurons generate action potential to trasmit information through the nervous system. Studying the single fiber recordings from the crab *Carcinus Maenas*, Hodgkin (1948) identified three different classes of excitability [1]. The classification scheme is still applied today bacause it encodes the fundamental characteristics of the generation of action potentials in neurons.
Class 1 axons are capable of firing repetively across a broad and continuous range of frequencies (5-150 spikes/s); class 2 axons can generate a repetitively response to a stimulus only in a narrower range (75-150 spikes/s); class 3 axons, instead, are not able to generate repetitive spiking.
In 1981, Catherine Morris and Harold Lecar proposed a model of excitability in barnacle muscles [2]. The Morris-Lecar model is particularly useful to study the excitability of neurons, mainly because it explains the Hodgkin's classification by using only two variables (namely the membrane voltage V and the fraction of open slowly-relaxing ion channel w - see **Model** section).
In the paper, we discuss the implementation of the Morris-Lecar model and we perform a one-parameter bifurcation analysis in order to see how it can reproduce the three classes of excitability identified by Hodgkin. The algorithm used are described in the section **Methods** and are available online (see **Supplementary Material**).

2 Model

The implementation of the model follows Ingalls [3]. Consider the membrane activity. Suppose changes in membrane voltage are due to two ionic currents: an inward calcium current and an outward potassium current and suppose that both calcium and potassium channels are voltage-dependent.
We can thus model the membrane activity with three variables, namely the membrane voltage V, the fraction of calcium and potassium open channels m and w. We call $m_\infty(V)$ and $w_\infty(V)$ the corresponding steady states, while $\tau_w(V)$ and $\tau_m(V)$ are the time *constants*. Let us call E_K and E_{Ca} the Nernst potential of potassium and calcium. Other parameters that should be introduced are the total capacitance of the membrane C (it is a measure of the membrane's ability to store a

charge difference) and the maximal membrane conductances g_{Ca} and g_K.
Morris and Lecar applied the following considerations:

- From experimental observations, it can be noticed that calcium channels relax to equilibrium much faster than potassium channels, thus the fraction m can be considered to be in steady-state approximation;
- Besides calcium and potassium, currents may be generated by other two sources. The first is a nonspecific leak current, which takes into account the activity of other ion fluxes; the second is an applied current I_{app} that describes any current injected into the cell.

From the previous considerations, the Morris Lecar model can be written as follows:

$$\frac{d}{dt}V(t) = \frac{1}{C}\left[\left(g_{Ca}m_\infty(V)\right)\left(E_{Ca} - V(t)\right) + g_K w(t)\left(E_K - V(t)\right) + g_{leak}\left(E_{leak} - V(t)\right) + I_{app}\right] \quad (1)$$

$$\frac{d}{dt}w(t) = \frac{w_\infty(V(t)) - w(t)}{\tau_w(V(t))} \quad (2)$$

The steady-state values for the gating variables m and w are given by

$$i_\infty(V) = \frac{1}{2}\left(1 + \tanh\left(\frac{V - V_i^*}{\theta_i}\right)\right) \qquad i = m, w \quad (3)$$

where V_m^*, V_w^*, θ_m and θ_w are model parameters.
While Ingalls considers the time *constant* voltage-independent, we decided to follow Liu [4], thus we write the time *constant* as function of the voltage:

$$\tau_w(V) = \phi_w \frac{1}{\cosh\left(\frac{V - V_w^*}{2\theta_w}\right)} \quad (4)$$

The values of the parameters are taken from Liu [4] and we write them here:

$$\begin{array}{ccc} E_{Ca} = 50 \text{ mV} & E_K = -100 \text{ mV} & E_{leak} = -70 \text{ mV} \\ g_Ca = 20 \text{ mS/cm}^2 & g_K = 20 \text{ mS/cm}^2 & g_{leak} = 2 \text{ mS/cm}^2 \\ \phi_w = 0.15 & C = 2 \ \mu\text{F/cm}^2 & \\ \theta_m = 18 \text{ mV} & \theta_w = 13 \text{ mV} & V_w^* = -10 \text{ mV} \end{array}$$

The one-parameter bifurcation analysis is performed in the (I_{app}, V_m^*) plane. We will see in the section **Results and Discussion** that the value paramter V_m^* let us discriminate between excitability of classes 1, 2 and 3.

3 Methods

To integrate the system of differential equations composed by equations (1) and (2) we used a fourth order Runge-Kutta algorithm. To find the zeros of the system of differential equation (and thus to perform the bifurcation analysis), we also implemented a two-dimensional Newton algorithm. The algorithms implemented are available in the section **Supplementary Material**.

3.1 Runge Kutta Algorithm

The fourth order Runge Kutta algorithm implemented was tested for a simple model from Ingalls [3], namely the *passive membrane model*: a simplified version of the Morris Lecar model for which an analitical solution exists. The differential equation that describes the model is the following:

$$\frac{dy}{dt} = \frac{g}{C}(E - y) \quad (5)$$

and has as analitical solution the following expression:

$$y(t) = E - \exp\left(-\frac{g}{C}t\right)(E - y_0) \quad (6)$$

where y_0 is the initial condition $y(t = 0)$. We used here the parameters indicated by Ingalls [3]:

$$g = 0.0144\text{mS/cm}^2 \quad C = 0.98\ \mu\text{F/cm}^2 \quad E = -93.6\ \text{mV}$$

The Runge Kutta algorithm is applied to the model. The results are shown in figure 1 and shows a good agreement between the numerical and the analitical solution.

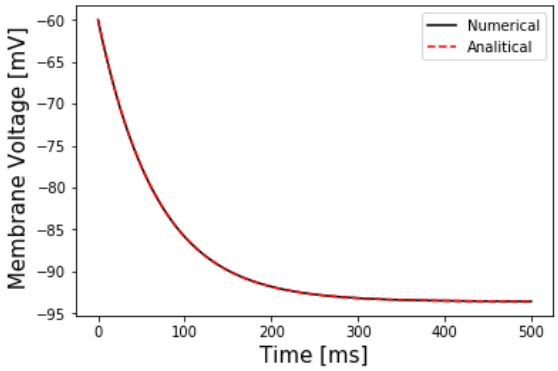

Figure 1: Runge Kutta algorithm applied to the passive membrane model (eq. 5) with parameters $g = 0.0144\text{mS/cm}^2, C = 0.98\ \mu\text{F/cm}^2$ and $E = -93.6$ mV. Time step $\Delta t = 0.1$ ms applied $Nstep = 5000$ times with initial conditions $y_0 = -60$ mV and $t_0 = 0$ ms

To quantify the agreement, we applied the algorithm using different time steps Δt and we calculated the global truncation error, i.e. the difference between the analitical and the numerical solutions. If the algorithm is correctly implemented, the error should be proportional to Δt^4. The results are fitted with a linear model and show the expected behaviour (figure 2).

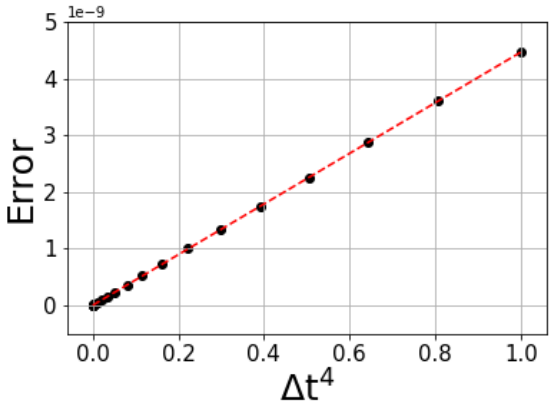

Figure 2: Global truncation error of the implemented fourth order Runge Kutta algorithm. The error is calculated for different time steps (black dots) and is fitted with a linear model with respect to the fourth power of the time step (red dashed line).

The linear dependence of the global truncation error with respect to the fourth power of the time step Δt shows that the algorithm was correctly implemented. To further check the algorithm, we performed some tests: the algorithm is applied forward and backward, thus we expect the final value to be the same as the initial one (within a certain tolerance); the algorithm is applied three times: first from time a to time c, then from time a to time b and from time b to time c (with $a < b < c$); the final values at time c should be equal (within a certain tolerance).
We then generalized the algorithm so that it is able to integrate not only a differential equation, but a system of ODEs. More information are available in the **Supplementary Material**

3.2 Newton Algorithm

In order to perform bifurcation analysis, we need to find the zeros of a function. The most known method to solve such a problem is the Newton algorithm, that needs the function and its derivative, toghether with an initail guess x_0.
To check the correctness of the implemented algorithm, we performed several tests. For example, for the test function

$$f(x) = x^2 - 4$$

the algorithm correctly finds as solution $x = \pm 2$ (for both $x_0 = 3.0$ and $x_0 = -1.5$).
Notice that if the function has more zeros, the algorithm should be applied several times, changing the initial guess x_0. We then generalized the Newton algorithm to two dimensions. In this case, the algorithm needs the set of functions and the Jacobian matrix. Of course, the initial value is a two-dimensional vector p_0.
The two-dimensional algorithm was tested with the set of functions

$$f(x, y) = 1 - 4x + 2x^2 - 2y^3 \qquad g(x, y) = -4 + x^4 + 4y + 4y^4$$

that has as zero the vector $(0.0617701, 0.724491)$, that is correctly found by the algorithm within a tolerance of 10^{-6} (starting vector $p_0 = (0.1, 0.7)$). Further information are available in the **Supplementary Material**.

3.3 Bifurcation Analysis

The one-parameter bifurcation analysis was applied as follows:

1. We set the value of the parameter V_m^* (chosen following Liu [4])
2. We set the value of I_{app}
3. We apply the two dimensional Newton algorithm to find the zeros of the Morris Lecar model composed by equations (1) and (2)
4. For each zero found, we calculate the eigenvalues[1] of the Jacobian matrix in that point to establish if the point is stable or unstable.
5. We change the value of I_{app}, covering the range 0:100.

The analysis is performed for three different values: $V_m^* = -23, -12, 0$ mV. For each value, we show the bifurcation diagram and the frequency plot. The frequency plot shows the frequency of the action potential[2] as a function of the applied current and let us distinguish between excitability of classes 1, 2 and 3. Further information are available in the **Supplementary Material**.

4 Results and Discussion

We performed the one-parameter bifurcation analysis taking three different values for the parameter V_m^*, according to the ones chosen by Liu [4]. We will see that according to the choice of the parameter, we are able to reproduce the three different classes of excitability.

4.1 Class 1 Neurons

First of all, we fix $V_m^* = -12.0$ mV. We apply the analysis as described in the **Bifurcation Analysis** section and we obtain the diagram in figure 3. We perform bifurcation analysis by changing the I_{app} parameter in the range 0:100.

[1] To calculate the eigenvalues, we used a function of the numpy library.

[2] To calculate the frequency of the potential, we analyze the signal as a function of time and we use the scipy function $find_peaks$ that let us determine the maxima of the signal. The difference between two adjacent maxima gives us the period of a function; the inverse of the period is the frequency.

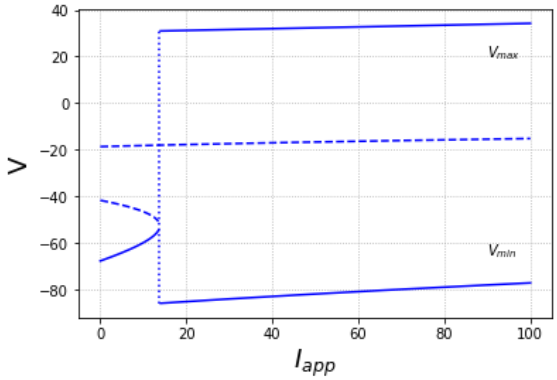

Figure 3: Bifurcation diagram for class 1 neurons: $V_m^* = -12.0$ mV. Dashed lines represent unstable points, while solid ones represent stable points. By increasing I_{app}, a saddle-node on invariant cycle (SNIC) bifurcation occurs; after the bifurcation, a limit cycle is generated. V_{max} and V_{min} represent the maximum and minimum values of the limit cycle.

The result is in agreement with literature (Liu [4] and Prescott [5]). From figure 3 it is possible to notice that, as I_{app} increases, the stable equilibrium (solid line) and the saddle equilibrium (curved dashed line) get nearer and nearer until a saddle-node bifurcation occurs. After the bifurcation, a stable limit cycle is generated. Because of the present of a third (unstable) equilibrium point (the almost horizontal dashed line), such a bifurcation is called saddle-node on invariant circle (SNIC) bifurcation.
From the bifurcation diagram, it is possible to notice two main behaviours of the neurons with the fixed parameter $V_m^* = -12.0$ mV. Examples of such behaviours are shown in figure 4.

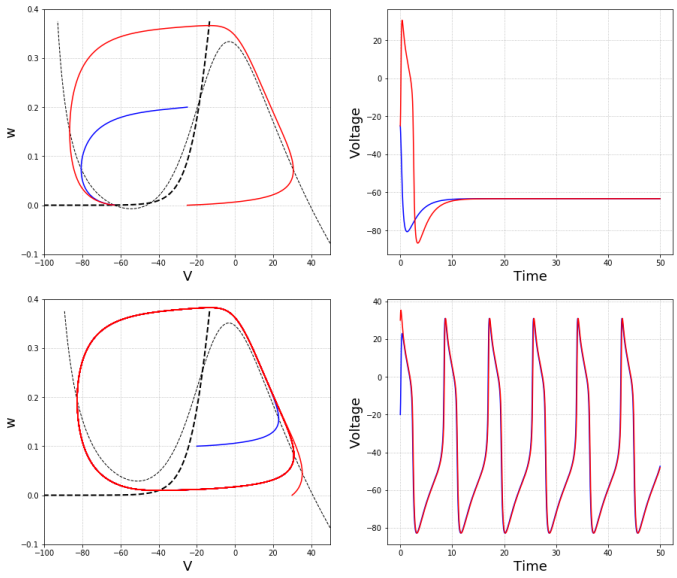

Figure 4: Examples of the behaviour of class 1 neurons under and above the SNIC bifurcation. On the left, we represent the phase space, while on the right we show the signal evolution in time. In the top image, the under-threshold behaviour is shown: no action potential is generated (we have only one spike). Parameters used: $I_{app} = 6.0$ mV; blue line: $V_0 = -25.0$ mV, $w_0 = 0.2$; red line: $V_0 = -25.0$ mV, $w_0 = 0.0$. In the bottom image, instead, the above-threshold behaviour is shown: a repetitive signal is generated and a limit cycle is formed in the phase space. Parameters used: $I_{app} = 40.0$ mV; blue line: $V_0 = -20.0$ mV, $w_0 = 0.1$; red line: $V_0 = -30.0$ mV, $w_0 = 0.0$. Light and heavy dashed lines in the phase space indicate V- and w-nullclines of the model.

Figure 4 shows that the action potential (repetitive firing) is generated above a certain threshold, corresponding to the SNIC bifurcation. This property is typical of neurons of classes 1 and 2. In order to distinguish between these two classes, we should look at the frequency plot (figure 5).

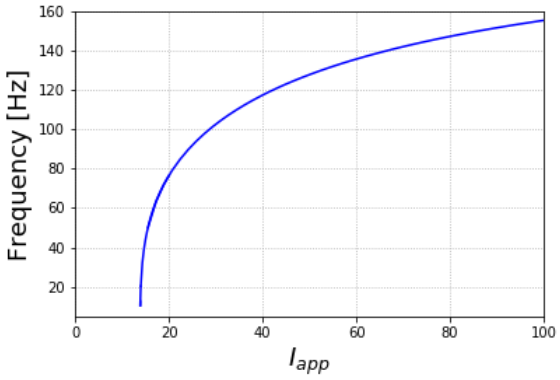

Figure 5: Frequency plot for $V_m^* = -12.0$ mV. The generated signal covers a broad range of frequencies: approximately from 10 to 160 Hz. This feature is typical of class 1 excitability.

As we can see from figure 5, the frequency of the generated action potential (above the SNIC bifurcation) can vary over a broad range, approximately from 10 to 160 Hz. Notice that Liu [4] and Prescott [5] demonstrated that the frequency can get down to zero and thus the plot is continuous. Our results are not in disagreement with respect to literature: for lack of computing power, we decided to exploit *only* 500 I_{app} values.
We conclude that setting the parameter to $V_m^* = -12.0$ let us discriminate class 1 neurons: in fact, the frequency plot (fig. 5) shows that the generated signal covers a broad range of frequencies.

4.2 Class 2 Neurons

We now set the parameter $V_m^* = 0.0$ mV and we perform the analysis described in the **Bifurcation Analysis** section. By varying the applied current I_{app} in the range 0:100, we obtain the bifurcation diagram shown in figure 6.

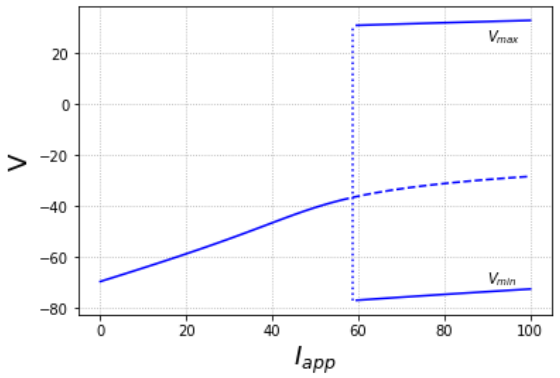

Figure 6: Bifurcation diagram for $V_m^* = 0.0$ mV. Dashed line correspond to unstable points, while solid lines represent stable equilibrium points. At $I_{app} \approx 57$, a Hopf bifurcation occurs: the stable point becomes unstable and a limit cycle is generated. V_{max} and V_{min} represent respectively the maximum and minimum values of voltage of the limit cycle. This behaviour is typical of class 2 excitability.

If the applied current is relatively small, than the Morris-Lecar model has one stable equilibrium point (solid line in figure 6). Approximately at $I_{app} = 57$, a Hopf bifurcation occurs: the stable point becomes unstable and a limit cycle is generated. Thus, we can distinguish two behaviours

for this kind of neurons: two examples are shown in figure 7.

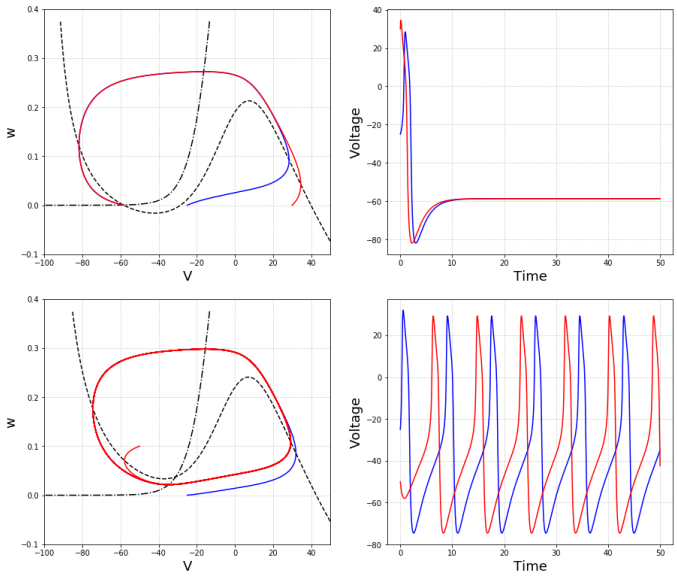

Figure 7: Examples of the behaviour of the model under and above the Hopf bifurcation. On the left, we represent the phase space; on the right, the signal evolution in time. In the top image, the under-threshold behaviour is shown: no potential action is generated and the model reaches a stable point in the phase space. Parameters used: $I_{app} = 20.0$ mV; blue line: $V_0 = -25.0$ mV, $w_0 = 0.0$; red line: $V_0 = 30.0$ mV, $w_0 = 0.0$. In the bottom image, the above-threshold behaviour is generated: action potentials are generated with different frequencies and a limit cycle is formed in the phase space. Parameters used: $I_{app} = 80.0$ mV; blue line: $V_0 = -25.0$ mV, $w_0 = 0.0$; red line: $V_0 = -50.0$ mV, $w_0 = 0.1$. Light and heavy dashed lines in the phase space indicate V- and w-nullclines of the model.

As visible in the examples in figure 7, the class 2 excitability, as class 1, provides two possible behaviours: under a certain threshold, the action potential is not generated and the signal has only one spike; above the threshold, that here corresponds to the Hopf bifurcation, the action potential is generated, several spikes with different frequencies can be generated and a limit cycle is formed in the phase space.
Again, to distinguish between class 1 and class 2 neurons, we need the frequency plot (figure 8).

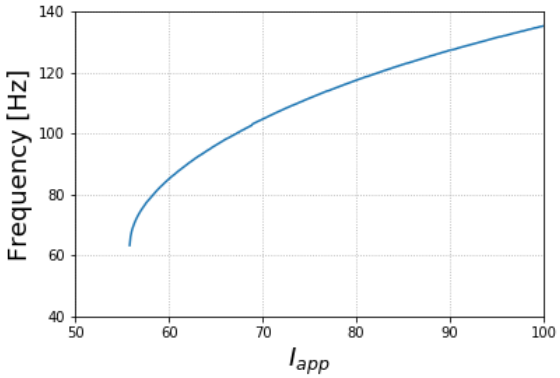

Figure 8: Frequency plot for $V_m^* = 0.0$ mV. The generated action potential covers a narrow range of frequencies, approximately from 60 to 140 Hz. This characteristic is typical of class 2 excitability.

In order to appreciate the fact that the frequency plot is discontinuous for $V_m^* = 0.0$ mV, we decided to plot only the I_{app} range that goes from 50 to 100. As visible from figure 8, the model is not

able to generate action potential with arbitrarily small frequencies: the frequency range *available* is approximately 60:140 Hz.
Setting $V_m^* = 0.0$ mV, we obtain a model that has the typical behaviour of class 2 excitability: the frequency plot (figure 8) shows that the action potential generated cannot have arbitrarily small frequencies; in fact, the frequency range of the generated signal (60-140 Hz) is quite smaller than the one of class 1 excitability (10-160 Hz).
Before concluding this section, we have to notice that the model for $V_m^* = 0.0$ mV and near the Hopf bifurcation can show bistability, as shown in figure 9. This is due to the fact that in a narrow range of I_{app} values near the Hopf bifurcation, a particular kind of bifurcation, namely a tangent bifurcation, coexists with the limit cycle. We decide to show this behaviour for completeness, but since the range of values for which this behaviour occurs is very small, we will go no further.

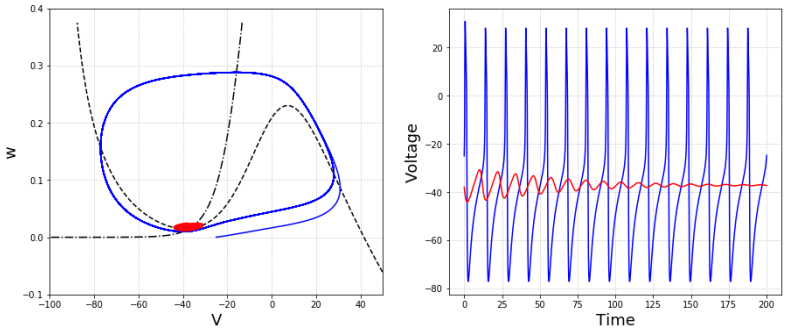

Figure 9: Example of the behaviour of the model for $V_m^* = 0.0$ mV near the Hopf bifurcation ($I_{app} = 57.0$). The model shows bistability: the blue line shows an action potential, while the red one relaxes to a stable point. Parameters used: blue line: $V_0 = -25.0$ mV, $w_0 = 0.0$; red line: $V_0 = -38.0$ mV, $w_0 = 0.025$. Light and heavy dashed lines in the phase space indicate V- and w-nullclines of the model.

4.3 Class 3 Neurons

Let us set $V_m^* = -23.0$ mV and perform the analysis as discussed in the **Bifurcation Analysis** section. As shown in figure 10, no bifurcation occurs: no matter the current applied to the neuron, it would never generate an action potential.

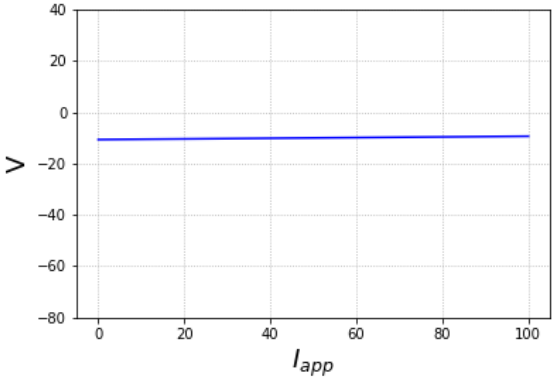

Figure 10: Bifurcation diagram for $V_m^* = -23.0$ mV. The solid line corresponds to the stable point reached by the model. No matter the value of the current I_{app}, the model shows no bifurcations. This behaviour is typical of class 3 neurons.

5 Conclusions

We discussed how the Morris-Lecar model can be used to distinguish between neurons with excitability of classes 1, 2 and 3. In particular, by changing the parameter V_m^* in the model and by performing a bifurcation analysis on the I_{app} parameter, we are able to associate to a value of the parameter V_m^* the Hodgkin's class of the neuron considered.
We have seen that setting $V_m^* = -12.0$ mV, we obtain the features typical of class 1 excitability, i.e. that the action potential is generated above a certain threshold, that corresponds to a SNIC bifurcation (figure 3), and the generated signal can cover a broad range of frequencies (figure 5).
Setting $V_m^* = -12.0$ mV, we obtain the characteristics of class 2 excitability: the action potential is generated above a certain threshold, that corresponds to a Hopf bifurcation (figure 6) and the generated signal can cover a narrower range of frequencies with respect to class 1 neurons (figure 8). We also noticed that near the Hopf bifurcation, the model shows bistability (figure 9).
For what concerns class 3 neurons, we set $V_m^* = -23.0$ mV and we obtain that no bifurcation occurs in the model (figure 10).
To further investigate the model, we could choose a whole set of values for V_m^* (e.g covering the range from -25 mV up to 5 mV) to obtain a two-parameter bifurcation diagram. Alternatively, we could choose to fix the V_m^* paramter and perform the bifurcation analysis in the (I_{app}, V_w^*) plane, as reported by Liu [4].

Supplementary Material

All the codes (algorithms, tests, data analysis) are implemented in Python and are available in the following github repository:

https://github.com/michelestofella/morris

Bibliography

[1] Hodgkin A. (1948), *The local electric changes associated with repetitive action in a non-medullated axon*, J Physiol 107; 165-181
[2] Morris C., Lecar H., (1981), *Voltage oscillations in the barnacle giant muscle fiber*; Biophysical Journal, 35, 193-231
[2] Ingalls P., *Mathematical Modeling in Systems Biology. An Introduction*, MIT Press (2013)
[3] Liu X., *Bifurcation Analysis of a Morris-Lecar Neuron Model*, Biological Cybernetics (2014)
[5] Prescott S.A. (2014) Excitability: Types I, II, and III. In: Jaeger D., Jung R. (eds) Encyclopedia of Computational Neuroscience. Springer, New York, NY